# Global properties of even-even superheavy nuclei in macroscopic-microscopic models

Andrzej Baran,[1] Zdzisław Łojewski,[2] Kamila Sieja,[1,3] and Michał Kowal[4]
[1]*Institute of Physics UMCS, Radziszewskiego PL-10, 20-031 Lublin, Poland*
[2]*Institute of Informatics UMCS, Pl. M. Curie-Skłodowskiej 1, 20-031 Lublin, Poland*
[3]*Centre d'Etudes Nucléaires de Bordeaux Gradignan, Le Haut Vigneau BP120, F-33175 Gradignan, France*
[4]*The Andrzej Sołtan Institute for Nuclear Studies, Hoża PL-69, 00-681 Warsaw, Poland*
(Received 17 May 2005; published 26 October 2005)

A systematic study of global properties of superheavy nuclei in the framework of macroscopic-microscopic method is performed. Equilibrium deformations, masses, quadrupole moments, radii, shell energies, fission barriers and half-lives are calculated using the following macroscopic models: Myers-Swiatecki liquid drop, droplet, Yukawa-plus-exponential, and Lublin-Strasbourg drop. Shell and pairing energies are calculated in Woods-Saxon potential with a *universal* set of parameters. The analysis covers a wide range of even-even superheavy nuclei from $Z = 100$ to 122. Magic and semimagic numbers occurring in this region are indicated and their influence on the observables is discussed. The strongest shell effects appear at proton number $Z = 114$ and at neutron number $N = 184$. Deformed shell closures are found at $N = 152$ and 162. Spontaneous fission half-lives are calculated in a dynamical approach where the full minimization of the action integral in a three-dimensional deformation space of $\beta$ deformations is performed. The fission half-lives obtained this way are two orders of magnitude smaller than the ones resulting from static calculations. The agreement of theoretical results and experimental data is satisfying.

DOI: 10.1103/PhysRevC.72.044310 PACS number(s): 25.85.Ca, 23.60.+e, 21.10.Tg, 21.10.Ft

## I. INTRODUCTION

Since the successful production of superheavy elements (SHE) $Z = 110, 111$, and 112 in GSI [1–3] the process of synthesis of nuclei belonging to the *island of stability* predicted theoretically in the 1960s [4–6] has been sped up. The $Z = 114$ element was reported by the Dubna group in 1999 [7] and only 2 years later the $Z = 116$ element was discovered [8]. Another significant achievement of nuclear experimentalist was the production of nine odd-proton number superheavy nuclei originating from the isotopes of the $Z = 115$ element [9]. The most recent discovery, belonging to the RIKEN scientists, was synthesizing the $Z = 113$ element [10]. Although all elements with $110 \leqslant Z \leqslant 116$ have been produced successfully in the laboratory, the experimental evidence is still far from being complete and the data that already exist are being still modified as a result of new experiments. Nevertheless, the fast progress in experimental techniques and intensive studies of the heaviest elements by different groups (Dubna, GSI, Jyväskylä, Livermore, RIKEN) promise to verify all the data independently in various laboratories.

These successful experimental efforts provide a great challenge for nuclear theory, not only in terms of interpretation of the measured data. What is expected as well is extrapolation of the theoretical results to the regions of nuclei not yet observed. Only the models able to reproduce the existing data to a high accuracy for a wide range of nuclei can be considered reliable for predictions of properties of nuclei not known and to explain the physics underlying the observed phenomena.

The theoretical investigation of the superheavy region has been as well very intense in recent years. In searching for the *island of stability* and the next doubly magic nucleus many of approaches were employed by different authors, e.g., fully self-consistent calculations such as Skyrme-Hartree-Fock (SHF) [11] or the relativistic mean-field (RMF) model [12,13] and on the other hand Strutinsky-like calculations with more refined macroscopic-microscopic (MM) formulas such as the finite range droplet model (FRDM) [14], Yukawa-plus-exponential (YpE) [15], or the recent Lublin-Strasbourg drop (LSD) [16,17]. Different approaches, however successful in determining of some properties of studied superheavy nuclei, are not fully consistent in their predictions of, e.g., magic numbers beyond the well-known $Z = 82$ and $N = 126$. The major magic proton number $Z = 114$ indicated in MM calculations was also found in the RMF model with NL-SH parametrization [18]. However, Skyrme-Hartree-Fock calculations do not support this prediction, anticipating the shell closure instead at $Z = 124, 126$ [19]. Several models agree that a shell gap should occur at the neutron number $N = 184$ but various RMF calculations predict no strong shell effects for this number [20].

The differences in the description of shell effects are followed by various predictions of deformation properties of superheavy nuclei. The recent RMF results [20] suggest shape coexistence and superdeformed minima for the heaviest nuclei, whereas the MM approaches disfavor any superdeformation [21]. The disagreements between MM and fully microscopic approaches as well as the differences in predictions of the same type of calculations depending on the parameter sets used should be clarified basing on the available experimental data.

In the present work we perform a detailed study of nuclear properties calculated in various MM approaches for a wide range of even-even superheavy nuclei with $Z = 100$–122. Considering this region our article overlaps the formerly published studies of that type done by the Warsaw group [22–24],

 

where a similar range of SHE was studied in the YpE+WS model. Here, the commonly used macroscopic models such as Myers-Swiatecki drop (MSD), the droplet model (DPT) [25], or Yukawa-plus-exponential [26] are examined in comparison to the recent (LSD) model, which was shown to be more powerful in determining masses and fission barriers all over the periodic table [27,28]. The microscopic corrections to the liquid drop energy are calculated in Woods-Saxon potential with a *universal* set of parameters [29].

The outline of the present work is as follows. In Sec. II we present the theoretical background of our calculations. We briefly review the recent LSD model and then discuss the methods employed to determine half-lives of considered nuclei. Some calculational details are given in Sec. II C. Section III is devoted to presentation of our results and consists of three parts. First, we discuss equilibrium deformations, radii, and shell and pairing corrections based on the LSD model (Sec. III A). In Sec. III B we focus on the effects of different macroscopic models on properties of superheavies, e.g., on $\alpha$-decay energies, fission barriers heights, and lifetimes. Finally, in Sec. III C we verify the results by comparison to available experimental data. Concluding remarks are collected in Sec. IV.

## II. THEORETICAL MODEL

The total binding energy in the macroscopic-microscopic method is obtained as a sum of a smooth energy based on a liquid drop type formula and shell plus pairing corrections. Because the Strutinsky-type calculations are well known and most of macroscopic models used in the presented study were widely discussed in the literature, let us only briefly review the LSD formula in the next section.

### A. Lublin–Strasbourg drop

The nuclear mass according to the curvature-dependent LSD model proposed in Ref. [27] is given by the following formula:

$$\begin{aligned} M(Z,N;\mathrm{def}) = {} & ZM_H + NM_n - 0.00001433Z^{2.39} \\ & + b_{\mathrm{vol}}\,(1-\kappa_{\mathrm{vol}}\,I^2)\,A \\ & + b_{\mathrm{surf}}\,(1-\kappa_{\mathrm{surf}}I^2)\,A^{2/3}B_{\mathrm{surf}}(\mathrm{def}) \\ & + b_{\mathrm{cur}}\,(1-\kappa_{\mathrm{cur}}\,I^2)\,A^{1/3}B_{\mathrm{cur}}(\mathrm{def}) \\ & + \frac{3}{5}e^2\frac{Z^2}{r_0^{\mathrm{ch}}A^{1/3}}B_{\mathrm{Coul}}(\mathrm{def}) - C_4\frac{Z^2}{A} \\ & + E_{\mathrm{micr}}(Z,N;\mathrm{def}) + E_{\mathrm{cong}}(Z,N), \end{aligned} \quad (1)$$

where

$$E_{\mathrm{micro}} = E_{\mathrm{pair}} + E_{\mathrm{shell}} \quad (2)$$

and

$$E_{\mathrm{cong}} = -10\,\mathrm{MeV}\exp(-42|I|/10) \quad (3)$$

is the congruence energy according to Ref. [30]. $B_x$ ($x =$ surf, cur, Coul) are coefficients that depend on the geometry of the nuclear shape and are defined as the ratio of corresponding energies of a deformed and a spherical nucleus

$$B_x = \frac{E_x(\mathrm{def}\neq 0)}{E_x(\mathrm{def}=0)}. \quad (4)$$

Definitions of the curvature ($B_{\mathrm{cur}}$), Coulomb ($B_{\mathrm{Coul}}$), and surface ($B_{\mathrm{surf}}$) coefficients remain the same as in the standard drop model (Coulomb and surface coefficients) or in the droplet model (curvature coefficient $B_{\mathrm{cur}}$) [25,31]. The parameters appearing in Eq. (1) are as follows:

$$\begin{aligned} b_{\mathrm{vol}} &= -15.4920\,\mathrm{MeV}, \\ \kappa_{\mathrm{vol}} &= 1.8601, \\ b_{\mathrm{surf}} &= 16.9707\,\mathrm{MeV}, \\ \kappa_{\mathrm{surf}} &= 2.2938, \\ b_{\mathrm{cur}} &= 3.8602\,\mathrm{MeV}, \\ \kappa_{\mathrm{cur}} &= -2.3764, \\ r_0 &= 1.21725\,\mathrm{fm}, \\ C_4 &= 0.9181\,\mathrm{MeV}. \end{aligned}$$

Such a liquid drop formula with microscopic corrections as in Ref. [32] results in root-mean-square (rms) mass deviations equal to 0.698 MeV for binding energies of 2766 nuclei with $Z \geqslant 8$ and $N \geqslant 8$ and rms = 0.88 MeV for 40 fission barrier heights experimentally known.

### B. Spontaneous fission and $\alpha$-decay half-lives

At the present stage, there is still no fully microscopic approach to nuclear fission. Theoretical works of the self-consistent type focus mostly on extracting the fission barriers but the serious drawback of this type of calculations is overestimating the barrier heights. There are still not many studies of nuclear dynamics and collective motion described in a completely microscopic way. The work of Ref. [33], where time-dependent calculations based on the generator coordinate method and Hartree-Fock-Bogoliubov states were performed, has been recently developed [34] to calculate the kinetic energy distribution and mass distribution of fission fragments of $^{238}$U. However, it is not easy to predict fission half-lives by use of such an approach. We describe the spontaneous fission of a nucleus as a tunneling through the many-dimensional collective potential energy barrier. In the WKB approximation the spontaneous fission half-life is inversly proportional to the probability $P$ of the penetrability through the barrier

$$T_{\mathrm{sf}} = \frac{\log 2}{n}\frac{1}{P}, \quad (5)$$

$n$ being the number of assaults of the nucleus on the fission barrier in a time unit. For a vibrational frequency $\hbar\omega_0 =$ 1 MeV assumed in this article one obtains $n = 10^{20.38}\,s^{-1}$.

The tunneling probability $P$ can be determined as [35]

$$P = (1 + e^{2S})^{-1}, \tag{6}$$

where $S(L)$ is the action integral calculated along the fission path $L(s)$ in the multidimensional space of deformations

$$S(L) = \int_{s_1}^{s_2} \left\{ \frac{2}{\hbar^2} B_{\text{eff}}(s)[V(s) - E] \right\}^{1/2} ds. \tag{7}$$

Here $s$ is the arc length measured along the curve $L$ and $E$ is the energy of the system. The effective inertia $B_{\text{eff}}(s)$ is given by the following:

$$B_{\text{eff}}(s) = \sum_{k,l} B_{kl}(\{\beta_\lambda\}) \frac{d\beta_k}{ds} \frac{d\beta_l}{ds}, \tag{8}$$

where $\{\beta_\lambda\}$ is the set of collective degrees of freedom. Collective tensor components $B_{kl}$ for multipole vibrations can be evaluated in the first-order perturbation approximation [36,37]

$$B_{kl}(\beta) = 2\hbar^2 \sum_m \frac{\langle 0|\partial/\partial\beta_k|m\rangle\langle m|\partial/\partial\beta_l|0\rangle}{\mathcal{E}_0 - \mathcal{E}_m}, \tag{9}$$

where $|0\rangle$ and $|m\rangle$ denote ground and excited states of a nucleus with the corresponding energies $\mathcal{E}_0$ and $\mathcal{E}_m$. For an even-even nucleus excited states can be described in terms of two-quasiparticle excitations $\mathcal{E}_m = E_\nu + E_\mu$. After the transformation to quasiparticles Eq. (9) takes a compact form [38,39]

$$B_{kl}(\beta) = 2\hbar^2 \sum_{\mu,\nu} P^k_{\mu\nu}(\beta)(E_\mu + E_\nu)^{-1} P^l_{\nu\mu}(\beta), \tag{10}$$

where for the shape deformations

$$P^k_{\mu\nu}(\beta) = \frac{\langle\nu|\partial H_{s.p.}/\partial\beta_k|\mu\rangle}{E_\mu + E_\nu}(u_\mu v_\nu + u_\nu v_u) - \frac{1}{2}\delta_{\mu\nu}\left(\frac{\Delta}{E^2_\nu}\frac{\partial\lambda}{\partial\beta_k} + \frac{e_\nu - \lambda}{E^2_\nu}\frac{\partial\Delta}{\partial\beta_k}\right). \tag{11}$$

Here $u_\mu$ and $v_\mu$ are BCS occupation amplitudes, $H_{s.p.}$ is the single-particle Hamiltonian with eigenvalues $e_\mu$ and $E_\mu = \sqrt{(e_\mu - \lambda)^2 + \Delta^2}$ is the quasiparticle energy corresponding to the state $|\mu\rangle$.

Theoretical investigations of spontaneous fission half-lives are usually based on the static approximation [40,41] or on the method connecting dynamical calculations in two-dimensional deformation space with the simultaneous minimization of the potential energy in the remaining degrees of freedom [22, 23,42]. The advantages of the dynamical treatment of fission process are the following. Contrary to the static calculations, where a phenomenological inertia function may be considered and at least one free parameter fitted to experimental data is present in the analysis, in the dynamical approach we have no adjustable parameters of this type. The second issue is that phenomenological mass tensor disregards the shell structure of a nucleus, whereas in the dynamical treatment of fission process it is taken into account in calculations of the effective inertia tensor.

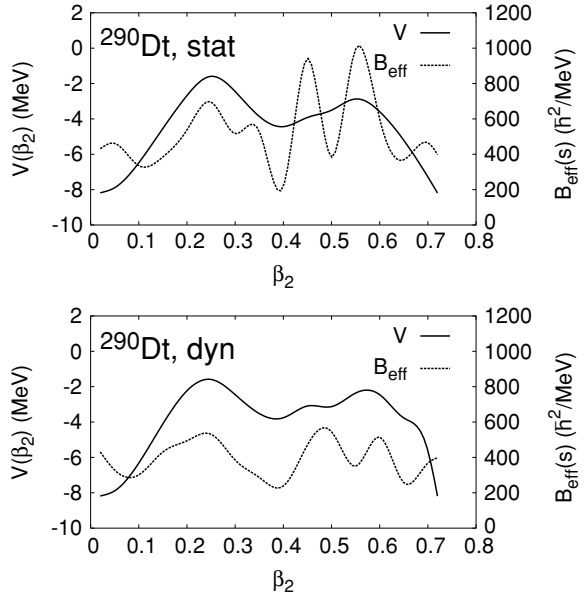


FIG. 1. Statical (stat) and dynamical (dyn) fission barriers $V(\beta_2)$ (MeV) (solid lines) and effective inertia $B_{\text{eff}}$ ($\hbar$/MeV) (dashed lines) as functions of elongation parameter $\beta_2$ calculated for $^{290}$Dt along statical and dynamical paths to fission discussed in the text. The left abscissa corresponds to the fission barrier and the right one to the mass parameter.

In the following, to find the trajectory $L_{\min}$ that fulfills a principle of stationary action [39]

$$\delta S(L) = 0 \tag{12}$$

we have used the multidimensional dynamical programming method first applied to fission in Ref. [43]. The algorithm of minimization searches all possible paths joining both the entrance of the barrier and the exit point and crossing all the grid points. This is performed in one pass, the cost of which is proportional to the dimension of the net. The classical entrance and exit points are defined by the equation $V(\{\beta_\lambda\}) = E \equiv E(\{\beta^0_\lambda\})$, where $\{\beta^0_\lambda\}$ are the ground-state deformations.

The above procedure leads in effect to a large decrease of the mass parameter as compared to the one calculated along a static path to fission and then to the increase of the fission probability and consequently to the decrease of the fission half-life $T_{\text{sf}}$. The behaviors of the effective inertia parameter $B_{\text{eff}}$ [see Eq. (8)] and the fission barrier $V(\beta_2)$ for $^{290}$Dt can be seen in Fig. 1. There are shown the cases calculated along statical and dynamical paths to fission as functions of elongation parameter $\beta_2$. In the case of dynamical path one sees a large reduction of the effective inertia as compared to the statical case. Typically, the values obtained along the dynamical path to fission are a factor of two smaller than the corresponding statical values. At the same time the barrier increases by about 10%. Correlations between the fission barrier and the mass parameter reflect the shell structure of the single-particle energies. Extrema of the potential energy and the inertia tensor nearly coincide.

From the phenomenology of $\alpha$ decay one knows that the half-life of an $\alpha$-particle emitter depends strongly on the energy ($Q_\alpha$) released in the process

$$Q_\alpha(Z,N) = B(Z,N) - B(Z-2,N-2) - B(2,2), \quad (13)$$

where $B(N,Z)$ is the binding energy of a nucleus with $Z$ protons and $N$ neutrons. In the literature there exist many phenomenological formulas describing the half-life of a nucleus with respect to an $\alpha$-particle emission. The parameters of these semiempirical approaches are fitted to available experimental data. In our study we follow the well-known equation of Viola and Seaborg [44]

$$\log T_\alpha = \frac{A_Z}{\sqrt{Q_\alpha}} + B_Z + C, \quad (14)$$

where

$$\begin{aligned} A_Z &= a_z\, Z + a_0 \\ B_Z &= b_z\, Z \end{aligned} \quad (15)$$

but with the parameters for $a_z$, $a_0$, $b_z$, and $C$ given in Ref. [45], where more experimental data were taken into account.

### C. Calculational details

Our calculations were done by use of the BCS approach, in the constant gap approximation with intensities $G_n, G_p$ following the dependences

$$\begin{aligned} G_n\, A &= 19.3 - 0.084(N-Z), \\ G_p\, A &= 13.3 + 0.217(N-Z), \end{aligned} \quad (16)$$

found in Ref. [46] and used successfully in the SHE region [41]. The pairing problem was solved in a truncated single-particle space taking into account $Z$ levels for protons and $N$ levels for neutrons in BCS equations.

The deformations are introduced as proportionality coefficients of the nuclear surface expansion

$$R(\theta) = R_0\, c\,(\{\beta_\lambda\}) \sum_{\lambda=2,4,6} [1 + \beta_\lambda Y_{\lambda 0}(\cos\theta)]\,, \quad (17)$$

where $c(\{\beta_\lambda\})$ is a constant calculated from the volume conservation condition, $R_0$ is the radius of equivalent spherical sharp density distribution ($R_0 = r_0 A^{1/3}$), and $Y_{\lambda 0}(\cos\theta)$ are spherical harmonics.

The potential energy and all the components of the inertia tensor were evaluated separately for each nucleus on a three-dimensional deformation grid defined as follows

$$\begin{aligned} \beta_2 &= 0\,(0.05)\,1.2, \\ \beta_4 &= -0.12\,(0.04)\,0.32, \\ \beta_6 &= -0.12\,(0.04)\,0.12. \end{aligned} \quad (18)$$

We disregard odd-multipolarity deformations ($\beta_3, \beta_5$) that play an important role only for lighter nuclei with more complex fission barriers [47]. In the case of heavy nuclei odd-multipolarities show up at a rather large quadrupole deformation $\beta_2 \sim 0.65$ that is close to the exit point (the end of the fission barrier). Therefore, their influence on the ground-state properties, $\alpha$ decay, and fission process is negligible. The dynamical treatment of fission allows us to neglect as well axially asymmetric shapes ($\gamma \neq 0$), the reason being that the effective inertia [Eq. (8)] is usually considerably larger along nonaxial trajectories than for those along $\gamma = 0$ and leads to larger action integrals in case of nonaxial shapes [42].

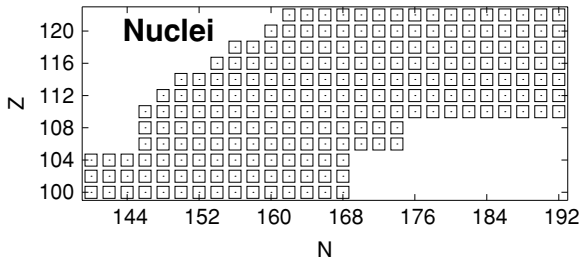


FIG. 2. The region of superheavy nuclei considered in the present study.

Having found the set of the ground-state deformations $\{\beta_2^0, \beta_4^0, \beta_6^0\}$ one can evaluate microscopically the quadrupole moments

$$Q_2 \equiv Q_{20}\big(\{\beta_\lambda^0\}\big) = \sqrt{\frac{16\pi}{5}} \sum_\nu \langle\nu|r^2 Y_{20}|\nu\rangle v_\nu^2, \quad (19)$$

where $|\nu\rangle$ are proton single-particle states in equilibrium point and $v_\nu^2$ are BCS occupation probabilities. Similarly, we can calculate the mean square charge radii:

$$\langle r^2\rangle_0 \equiv \big\langle r^2\big(\{\beta_\lambda^0\}\big)\big\rangle = \frac{1}{Z}\sum_\nu \langle\nu|r^2|\nu\rangle v_\nu^2 + 0.64\,\mathrm{fm}^2\,. \quad (20)$$

The last term here is the correction related to the finite range of the internal proton charge distribution.

## III. RESULTS

In the present work we consider the region of even-even superheavy nuclei that includes all up to now discovered SHE and additionally allows to study the structure of quantities crucial for their existence in a wide range of atomic ($Z = 100 \div 122$) and neutron numbers. Nuclei taken into account in our calculations are shown in Fig. 2. These are the superheavies that, according to our predictions, are still stable with respect to a proton or a neutron emission. This follows the analysis of single-particle separation energies ($S_p$, positively defined) that are positive for all described nuclear systems.

The results of our calculations are divided into three separate parts. First, we limit ourselves to the discussion of static nuclear properties (radii, quadrupole moments, shell energies) obtained only with the LSD model. In the second part we focus on the effects of different macroscopic models on the nuclear properties that strongly reflect the changes in the liquid drop energy, i.e., fission barrier heights, $\alpha$ decay, and spontaneous fission half-lives. In the last part we discuss in detail the LSD results and compare them to available experimental data.

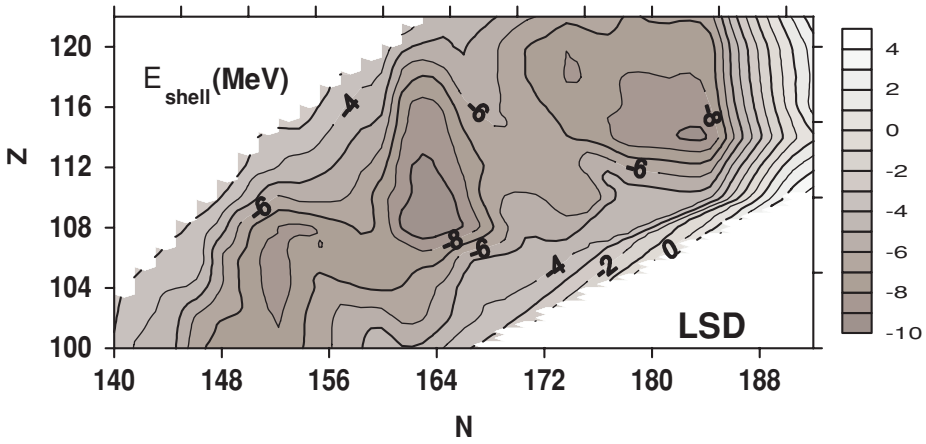


FIG. 3. Contour map of the Strutinsky shell energy ($E_{\text{shell}}$) for considered nuclei calculated in the ground state. The LSD model is used for the macroscopic part of the energy. The distance between isolines is 1 MeV.

### A. Static properties in the LSD model

In the following we discuss radii, quadrupole moments, and shell and pairing energies for studied nuclei. These properties are mostly dependent on the microscopic part of the energy and are affected by the smooth part only via its influence on the equilibrium deformation. The intermodel deviations of ground-state deformations are rather small, except in the case of the YpE model, where the maximal absolute deviation of elongation parameter $\beta_2$ reaches 0.08 and that of the hexadecapole deformation $\beta_4$ is equal to 0.04. It should be pointed out that despite the differences in equilibrium deformations predicted with various models the global behavior of the properties described in this section remains the same in all cases and possible differences concern only separate nuclei. Therefore, we restrict the discussion to the results of LSD model. Although the stability of SHE is determined mainly by shell effects, we begin this section with a discussion of shell energies.

#### *1. Shell correction*

Values of total shell energies $E_{\text{shell}}$ in ground states of considered nuclei are shown on a contour map in Fig. 3. Three minima of $E_{\text{shell}}$ are observed in this region. The first, of about $-8.5$ MeV, occurs for $N = 152$ for lighter superheavies and disappears for elements with $Z \geqslant 110$. The closure of the $N = 162$ subshell is represented by the second minimum ($-10$ MeV) for all isotopic chains. These strong shell effects form the island of well-deformed superheavy nuclei centered at $^{270}$Hs whose stability has been confirmed in recent experiments [48]. The last minimum ($-9.5$ MeV) shows up for $^{298}114$. This feature and the fact that all elements with $N = 184$ and $Z \geqslant 114$ have been predicted to have spherical shapes (see Fig. 5) suggests the magicity of the neutron number $N = 184$ and proton number $Z = 114$ that is in agreement with the results of other Strutinsky-type calculations [41] and of Skyrme-Hartree-Fock models [19].

#### *2. Mass*

In the region of superheavy nuclei the number of experimentally known masses is very limited. However, there exist estimates of nuclear mass obtained from the general trends [49,50]. Figure 4 shows the mass deviations $\Delta M = M_{\text{th}} - M_{\text{est}}$ in mega-electron volts for all reported estimates. The rms error for all known and estimated cases is $\sigma_{\text{mass}} = 0.51$ MeV. Maximal deviation does not exceed $\pm 1$ MeV. Similar results were obtained recently in the case of LSD+WS calculations with a more refined $\delta$-type pairing interaction (see Refs. [16,17]).

#### *3. Quadrupole moments*

In Fig. 5 we show quadrupole moments obtained accordingly to Eq. (19) within LSD calculations. It is seen that all the superheavy elements have prolate deformations whose magnitudes are slightly decreasing with the increase of the neutron number. An abrupt change of equilibrium deformation is clearly visible in isotopic chains of the heaviest elements in the vicinity of $N > 162$. The quadrupole moments in this region are suddenly lowered by a dozen or so units. The nuclei with $Z \geqslant 116$ and $N \geqslant 162$ are weakly deformed. Among

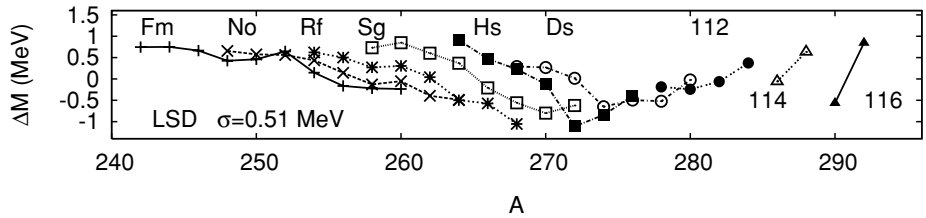


FIG. 4. Mass deviation $\Delta M$ (in mega-electron volts) resulting the calculations of Lublin-Strasbourg drop and Woods-Saxon model vs. mass number $A$. $\sigma$ denotes the rms error. Experimentally known masses and estimates were taken from Refs. [49,50].

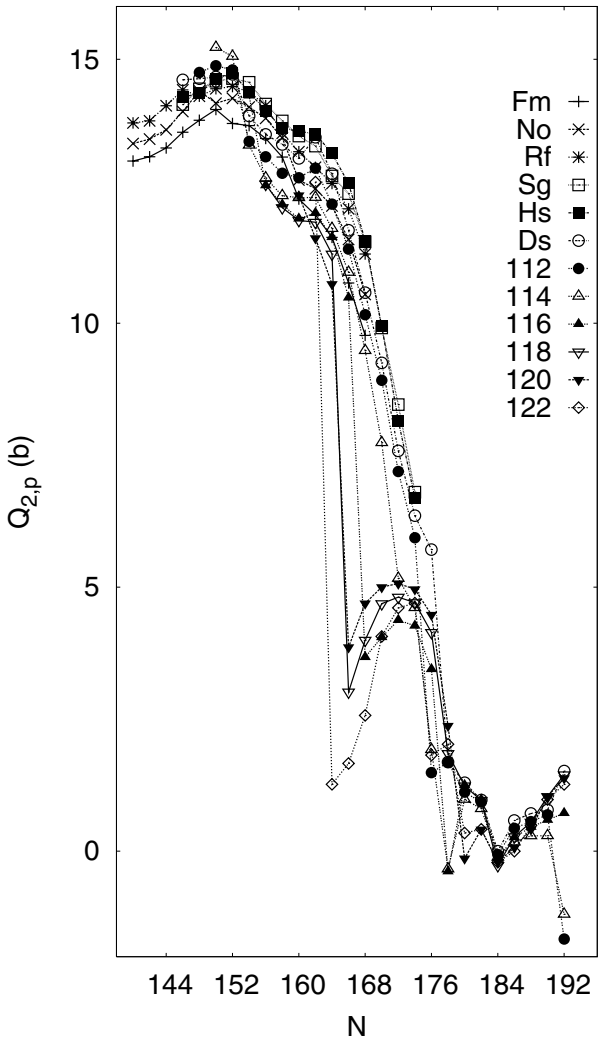


FIG. 5. Electric charge quadrupole moments ($Q_{2,p}$) in barns as a function of neutron number $N$. The underlying equilibrium deformations were calculated by use of the MM method with the LSD macroscopic part.

them, around the magic number $N = 184$, one observes a group of nuclei that tend to be spherical.

#### *4. Root-mean-square radii*

Root-mean-square charge radii [Eq. (20)] are shown in Fig. 6. A rather regular dependence of the radii on the neutron number is perturbed around $N = 162-166$, which can be attributed to the abrupt change of equilibrium deformation (see Fig. 5) that causes the difference in charge distribution. The local maxima in rms radii curves suggest that the Coulomb repulsion energy, approximately inversly proportional to the radius of the system, is locally smaller for these nuclei thus they are more stable. The nearly linear increase of the rms radii for the heaviest ($A \gtrsim 278$) nuclei is a consequence of their sphericity.

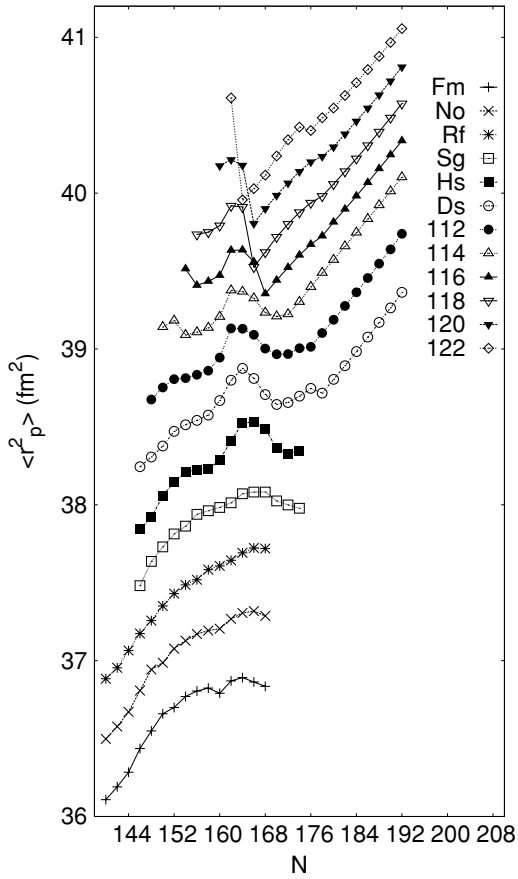


FIG. 6. Root-mean-square charge radii as functions of neutron number $N$ for even-even transfermium nuclei ($Z = 100 - 122$).

#### *5. Pairing gaps*

The shell structure is strongly reflected in the solutions of BCS equations. The BCS gap parameters ($\Delta_n$) for neutrons as a function of neutron number are displayed in Fig. 7. The values of $\Delta_n$ reach their maxima in the middle of shells and are significantly lowered when the shell effects become stronger. Additionally to the three distinct minima ($N = 152, 162, 184$) another one can be distinguished at $N = 174$. Zero values of pairing gaps around the shell closures are a drawback of the BCS method that does not provide superfluid solutions in cases of low-level density around the Fermi surface that is a consequence of the nonconservation of the particle number. One of the simplest method to cure this problem is applying the approach of Lipkin and Nogami (LN) [51,52]. The discussion of LN solutions as well as other particle number projection methods in the superheavy region will be given in a forthcoming publication [53].

### B. Decay properties in MM models

Decay properties of nuclei in this region of periodic table are determined by nuclear masses, the behavior of fission barriers and effective mass parameters. Energies released in

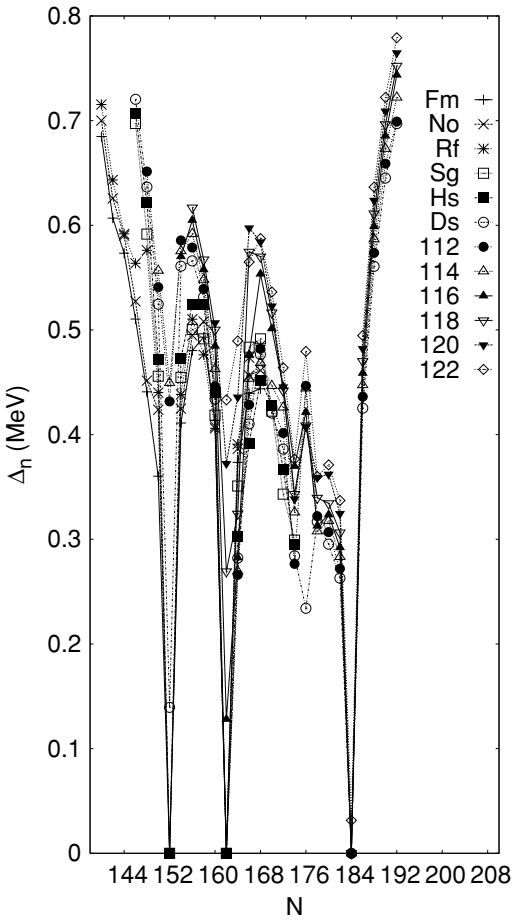


FIG. 7. Neutron pairing gap parameters ($\Delta_n$) in mega-electron volts resulting BCS calculations as a function of neutron number $N$. Each curve corresponds to one isotopic chain $Z = \text{const}$.

$\alpha$-particle emission which determine the half-lives with respect to this process are defined by the differences between nuclear masses of parent and daughter nuclei [Eq. (13)]. Contrary to $\alpha$ decay, the description of the fission process depends not only on the ground-state properties but as well on the shape of the fission barrier and mass tensor along the fission path. The behavior of barriers is decisive for the assesment of the macroscopic part of nuclear energy. In the following we compare the main quantities such as fission barrier heights and half-lives calculated in considered MM models.

#### *1. α-decay energies*

In the left part of Fig. 8 there are shown $\alpha$-decay energies ($Q_\alpha$) calculated with LSD. Experimental data of Ref. [49] are indicated by large open circles. The right panel of the figure shows the differences

$$\Delta Q_\alpha = Q_\alpha(\text{model}) - Q_\alpha(\text{LSD}), \tag{21}$$

in mega-electron volts, where the word *model* corresponds to the MSD, DPT, or YpE. As can be seen, the largest differences appear for the YpE model (up to 0.6 MeV). This leads to the estimated $\alpha$-decay half-lives that differ from the LSD results on $2-3$ orders of magnitude. Except the region with $N \sim 168$, where the deviations reach 0.3 MeV, the magnitudes of $Q_\alpha$ in the MSD, DPT, and LSD models are comparable. Consequently, the predictions of these models for $\alpha$-decay half-lives are similar. This is mainly the result of the fits of parametrizations of macroscopic models that are done in the ground states to the experimental nuclear masses. No role in this adjustment is played by heights and widths of fission barriers. It should be added that there are few reliable experimental evidences concerning the former and no data for the latter. Therefore, the significant differences between various MM models are expected in the case of dynamical quantities, such as fission half-lives.

#### *2. Fission barriers heights*

Figure 9 shows the heights of the first barrier $V_{\text{Bar}}$ for the LSD (left panel). Although this model appeared to be very successful in calculations of nuclear masses and barriers, we compare different results to those of the LSD. The differences are shown in the left part of the figure.

The barrier height ($V_B$) is defined as a difference of the barrier peak and the energy of the ground state, which is equal to the minimum of the macroscopic-microscopic energy. It is seen that the most significant differences (1 MeV) as compared to the LSD results occur when the YpE model is concerned. The MSD and DPT models give similar barrier heights that are, on avarage, 0.5 MeV lower for lighter superheavies and are in a good agreement with the LSD barriers for nuclei with $N \geqslant 168$. The results obtained in YpE model are the opposite—the barriers that are higher as compared to other models in the region of lighter superheavy nuclei become much lower with the increase of neutron number. An interesting fact is that the heights of the barriers become nearly the same (4–4.5 MeV) for elements around $N = 168$ that shows up in the corresponding similar stability of these nuclei with respect to spontaneous fission in all considered macroscopic models. This feature is a consequence of the fact that the shell energies of all nuclei with $N = 168$ are almost equal (see Figs. 3 and 9).

#### *3. Spontaneous fission half-lives*

Spontaneous fission half-lives ($T_{\text{sf}}$) calculated in the dynamical approach for LSD model are shown in the left part of Fig. 10. The half-life model differences with respect to LSD results for MSD, DPT, and YpE are shown in the right area of the figure.

The LSD model predicts the shortest half-lives for isotopic chains of lighter elements, namely fermium, nobelium, and ruthefordium. For these nuclei the estimates of the droplet model are up to 8 orders of magnitude larger, whereas for other nuclids the average deviation is about 2 orders of magnitude.

The half-lives predicted in the YpE drop are longer as compared to the LSD results in nearly all cases. These differences reach 4 orders of magnitude for $N$ less than

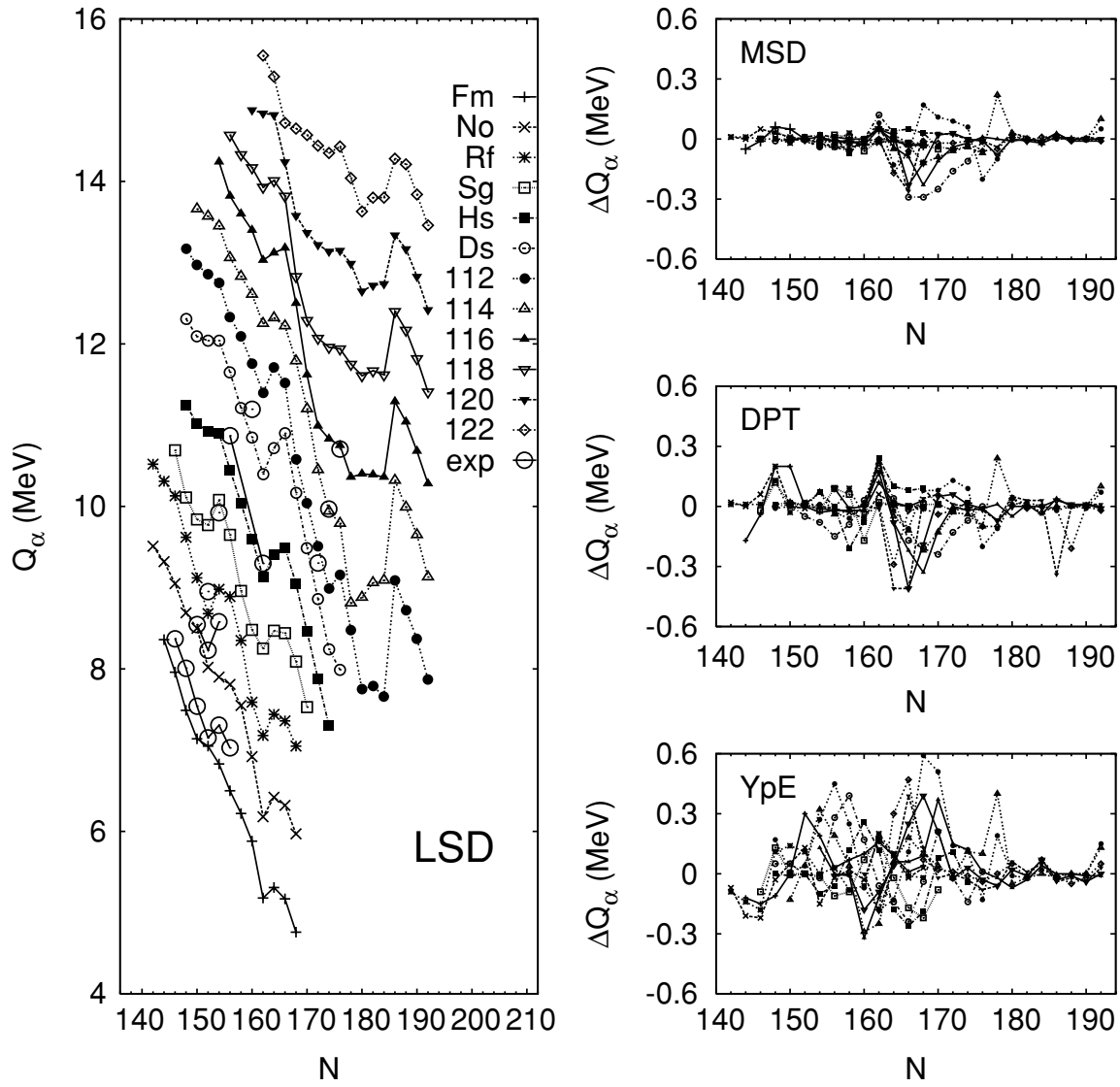


FIG. 8. $\alpha$-decay energies ($Q_\alpha$) in mega-electron volts calculated in the LSD model as functions of neutron number $N$ (left panel). Experimental values indicated by full circles come from Ref. [49]. The right panel shows the differences $\Delta Q_\alpha = Q_\alpha(\text{model}) - Q_\alpha(\text{LSD})$ in mega-electron volts where model corresponds to the MSD, DPT, and YpE. The symbols used for different isotopic chains are the same in all parts of the figure.

170, whereas in the case of heavier nuclei they are reduced approximately to 1 order of magnitude.

The largest half-lives are obtained with the use of the MSD model, which is known to give relatively high and wide fission barriers [54]. The average difference is around 4 orders of magnitude.

A characteristic feature that shows up in the case of all light nuclids ($Z \geqslant 112$) and all MM models is a large bump in half-life curves with a maximum at $N = 152$, which is a manifestation of the shell closure. For the same isotopic chains one observes a distinct plateau of $T_{\text{sf}}$ ranging from $N = 162$ to 168. The half-lives of heavier nuclei ($Z > 112$) are constantly increasing, reaching their maximal values at $N = 180$–184. After passing this point the curves fall down rapidly. The range of variation of $T_{\text{sf}}$ is very broad and covers 40 orders of magnitude. The behavior of half-lives reflects clearly the structure of the fission barrier heights (see Fig. 9) and is a consequence of shell effects.

### C. Decay properties in LSD model

Analyzing the half-lives of heavy and superheavy nuclei one should bear in mind the variation of data that reaches 40 orders of magnitude. The precision of model calculations should be very high to make the extrapolations reliable.

As it was already shown [16,17,27] the agreement of the LSD masses and experimental data is satisfactory and comparable to the results of self-consistent HFB models [55],

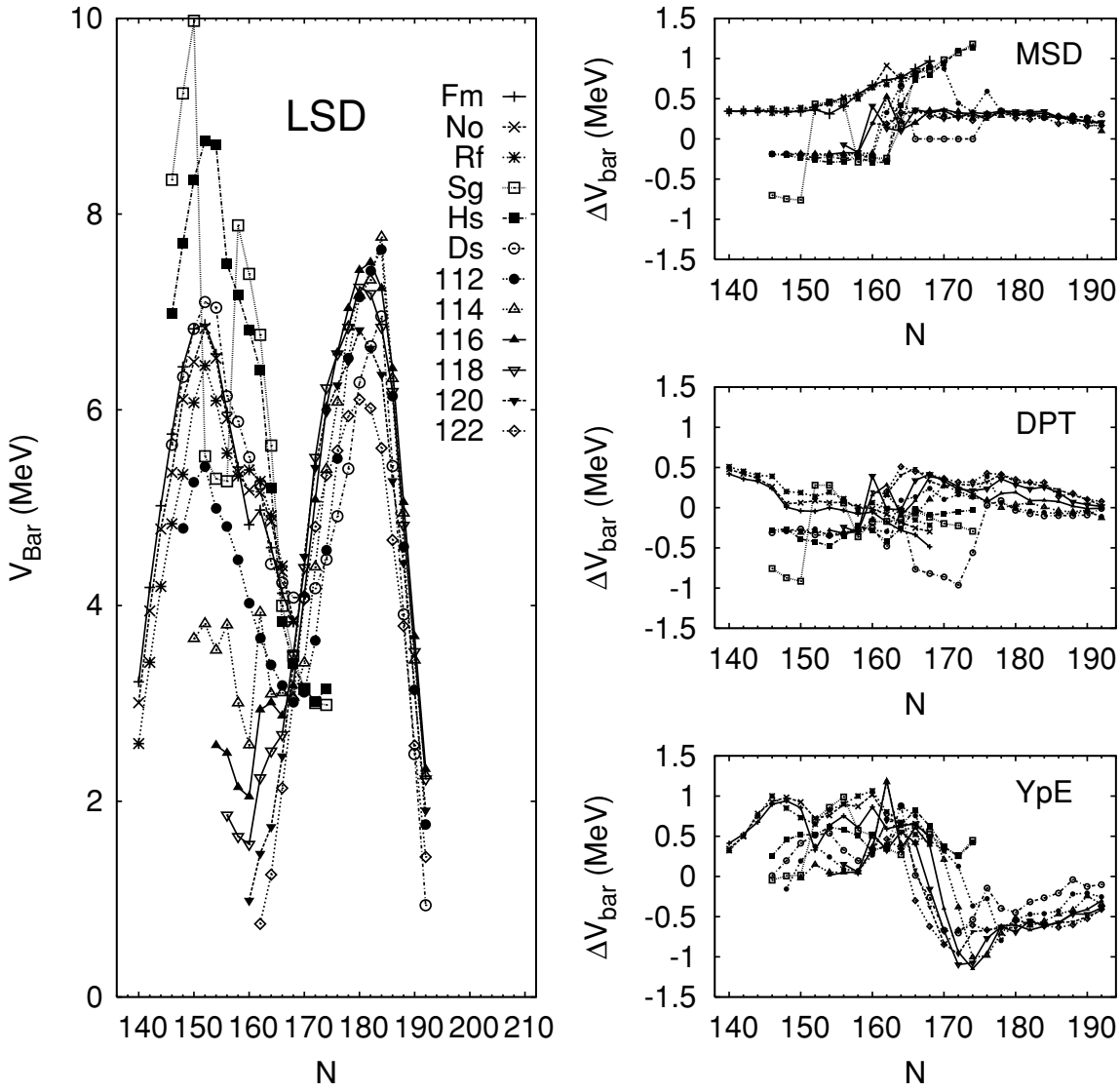


FIG. 9. First barrier heights (in mega-electron volts) versus neutron number $N$ for even-even nuclei with $Z = 100 - 122$. The left panel shows the results of calculations with macroscopic content corresponding to LSD model. The right panel shows the model deviations defined as $\Delta V_{\rm Bar} = V_{\rm Bar}(\text{model}) - V_{\rm Bar}(\text{LSD})$ where model corresponds to MSD, DPT, or YpE.

extended Thomas-Fermi approach [30], or FRDM [14]. The rms deviations for binding energy in all these models are $0.7 \pm 0.05$ MeV. Another important point is that because of a proper inclusion of the curvature term the fission barriers predicted in LSD model, especially in the region of heavier nuclei, are determined with a very high accuracy that is even better than that for the Thomas-Fermi approach. Therefore, and based on the discussion of Sec. III B, we expect the LSD model to be reasonable for predictions of half-lives and decay modes of SHE. However, the results for fission half-lives of fermium and nobelium isotopes obtained in YpE model are closer to experimental data.

#### *1. Spontaneous fission half-lives*

Looking at LSD results in Fig. 10 one can separate three sets of long-living nuclei. The first set is centered on $^{254}$No, which is the most stable within this group. The second region is formed by middle mass nuclei ($N \sim 162$) with $\log(T_{\rm sf}/{\rm y}) \sim -8$. The last group that is located in the vicinity of the magic number $N = 184$ contain nuclei with the longest fission half-lives $\log(T_{\rm sf}/{\rm y}) \sim 8$. However, it should not suggest the possibility of an easy experimental observation of these nuclei bacause other processes ($\alpha$ decay) may determine their existence.

#### *2. α-decay half-lives*

The range of $\alpha$-decay half-lives calculated from Eq. (14) is comparable to the one for spontaneous fission half-lives (Fig. 11). One observes a continous increase of the half-life with the kinks located at deformed subshell closures $N = 152$ and 162 and at the spherical $N = 184$ shell closure. The avarage slope of the $\log(T_\alpha/{\rm y})$ curves is larger for the

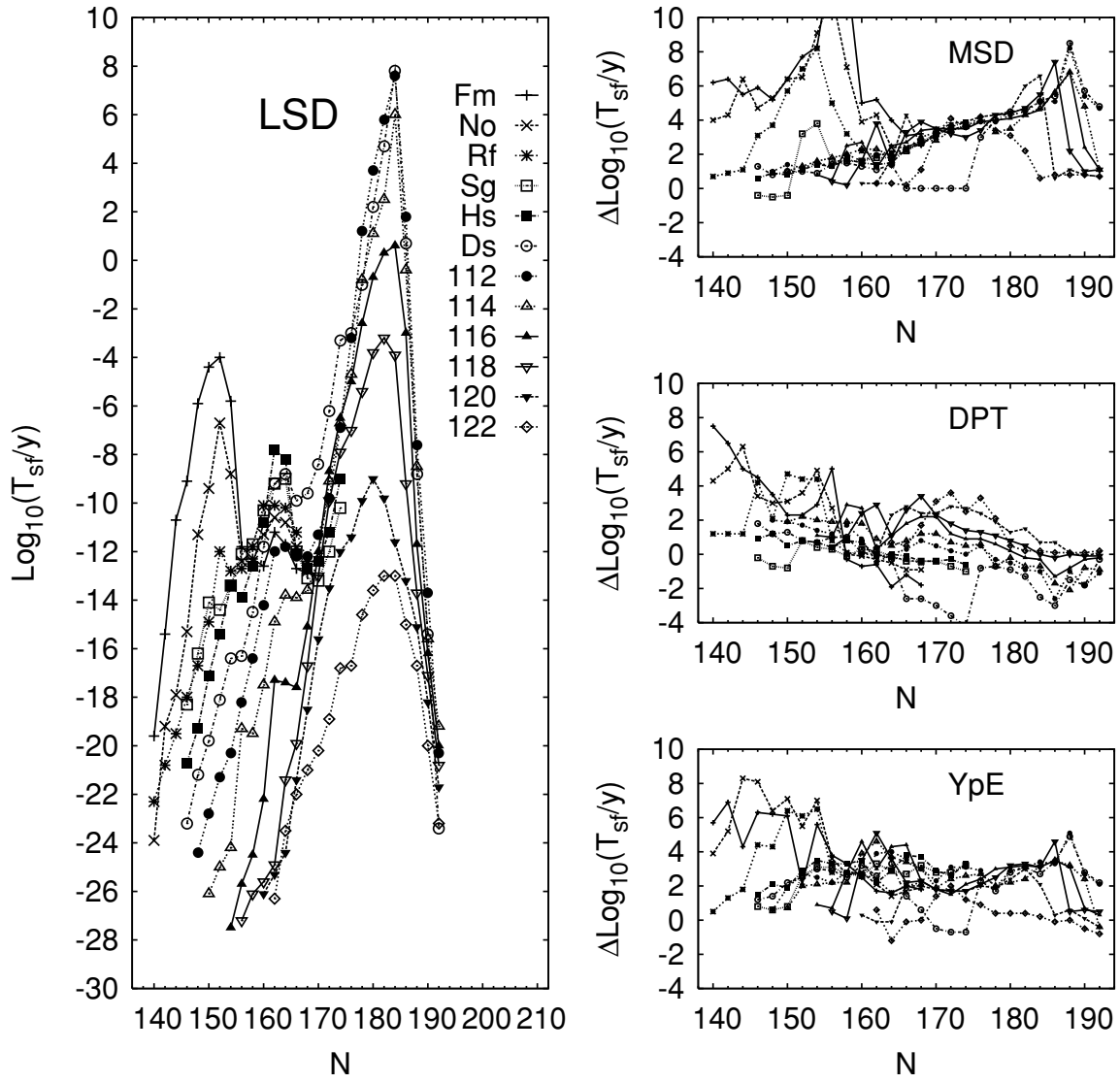


FIG. 10. The decimal logarithms of spontaneous fission half-lives (in years) calculated dynamically in LSD model (left panel). The right panel shows the deviations $\Delta \log_{10}(T_{\rm sf}/{\rm y}) = \log_{10}[T_{\rm sf}({\rm model})/{\rm y}] - \log_{10}[T_{\rm sf}({\rm LSD})/{\rm y}]$ where model corresponds to MSD, DPT, and YpE respectively.

nuclei with $Z \leqslant 114$ than of those with the atomic number greater than 114. As seen, the nuclids belonging to isotopic chains of lighter elements are resistant to an $\alpha$ decay, the lifetimes in this region are quite large contrary to the heaviest elements that are unstable with respect to an $\alpha$ decay ($A \geqslant 290$).

### 3. Decay probability

The last figure of this series (Fig. 12) shows the relative probability of $\alpha$ decay calculated as follows:

$$p_\alpha(\%) = 100 \frac{\Gamma_\alpha}{\Gamma_\alpha + \Gamma_{\rm sf}}, \tag{22}$$

where $\Gamma_\alpha$, $\Gamma_{\rm sf}$ are partial widths of $\alpha$ and spontaneous fission decays. The whole region of nuclei can be roughly divided into two parts. The first is of $\alpha$-decaying nuclids with $N \geqslant 170$ and $Z \geqslant 112$. The spontaneous fission is the dominant process for lighter nuclei. The approximate line of $A \sim 288$ crosses the area of the strongest competition between $\alpha$ and spontaneous fission decays.

### 4. Comparison to experimental data

Experimental investigation of SHE encounter a general problem that only a few atomic nuclei of each species are produced. In the region considered here, there are about 17 measured $Q_\alpha$ values and 30 total half-lives of even-even nuclei. For $Z \geqslant 110$ only seven cases are known. Therefore, the conclusions drawn from comparisons of theoretical and experimental data are slightly limited. However, good agreements of macroscopic-microscopic results in the

TABLE I. Results of LSD calculations vs. available experimental data taken from Refs. [49,50,59]. The first two column show atomic ($Z$) and neutron ($N$) numbers, respectively. The next column shows calculated values of electric charge quadrupole moment in barns. In the fourth and fifth columns we give calculated and experimental $\alpha$-decay energies in mega-electron volts. The decimal logarithms of total half-lives are given in columns six (theory) and seven (experiment). The last columns contain theoretical and experimental decay modes and intensities (in percentages). Asterisks indicate recent measurements of Dubna group [59].

| Symbol or $Z$ | $N$ | $Q_2$ (b) | $Q_\alpha$ (MeV) | $Q_\alpha^{\rm exp}$ (MeV) | $\log(T)$ | $\log(T^{\rm exp})$ | Mode(th) (%) | Mode(exp) (%) |
|---|---|---|---|---|---|---|---|---|
| Fm | 144 | 13.32 | 8.36 | | −10.70 | −9.98 | sf | sf ≈ 100 |
| | 146 | 13.61 | 7.96 | 8.37 | −9.10 | −7.45 | sf | sf4.5 |
| | 148 | 13.84 | 7.49 | 8.01 | −5.90 | −5.94 | sf | $\alpha$93 |
| | 150 | 14.04 | 7.14 | 7.54 | −4.40 | −4.24 | sf | $\alpha > 90$; sf0.0069 |
| | 152 | 13.78 | 7.05 | 7.15 | −4.00 | −2.54 | sf; $\alpha$2 | $\alpha$100 |
| | 154 | 13.74 | 6.83 | 7.31 | −5.80 | −3.43 | sf | $\alpha$100 |
| | 156 | 13.50 | 6.50 | 7.03 | −11.80 | −3.52 | sf | $\alpha$8.1; sf91.9 |
| No | 146 | 14.01 | 9.05 | | −15.30 | −13.1 | sf | |
| | 148 | 14.40 | 8.69 | | −11.30 | −12.7 | sf | sf ≈ 100 |
| | 150 | 14.16 | 8.50 | 8.54 | −9.40 | −7.11 | sf | $\alpha$67; sf32 |
| | 152 | 14.26 | 8.02 | 8.23 | −6.71 | −5.79 | sf; $\alpha$3 | $\alpha$90; sf0.17 |
| | 154 | 14.09 | 7.90 | 8.57 | −8.80 | −7.03 | sf | $\alpha$100; sf0.53 |
| Rf | 150 | 14.44 | 9.12 | | −14.90 | −11.13 | sf | $\alpha < 1.5$ |
| | 152 | 14.48 | 8.68 | 8.95 | −12.00 | −9.69 | sf | $\alpha$0.32 |
| | 154 | 14.38 | 8.98 | | −12.80 | −9.42 | sf | $\alpha$13; sf87 |
| | 156 | 14.12 | 8.89 | | −12.70 | −11.17 | sf | |
| | 158 | 13.60 | 8.35 | | −11.80 | −7.13 | sf | $\alpha < 0.8$; sf ≈ 100 |
| Sg | 152 | 14.63 | 9.77 | | −14.40 | −9.98 | sf | $\alpha < 20$ |
| | 154 | 14.56 | 10.08 | 9.92 | −13.40 | −9.92 | sf | $\alpha$40; sf60 |
| | 156 | 14.15 | 9.65 | | −12.10 | −7.13 | sf | $\alpha < 22$ |
| | 160 | 13.55 | 8.48 | | −10.30 | −6.17 | sf | $\alpha$34 |
| Hs | 156 | 14.02 | 10.45 | 10.87 | −13.90 | −10.76 | sf | $\alpha$50 |
| | 158 | 13.69 | 10.04 | 10.33 | −12.60 | −10.60 | sf | |
| | 162 | 13.59 | 9.13 | 9.29 | −7.83 | | sf; $\alpha$7 | |
| Ds | 160 | 13.12 | 10.85 | 11.20 | −11.83 | −11.29 | sf; $\alpha$8 | $\alpha$ 100 |
| 112 | 170 | 8.92 | 10.04 | | −11.30 | −10.49* | sf | sf* |
| | 172 | 7.20 | 9.51 | | −9.80 | −6.00 | sf | $\alpha$100 |
| | | | | | | −8.5* | | sf* |
| 114 | 172 | 5.17 | 10.45 | | −9.19 | −8.03* | sf; $\alpha$20 | $\alpha$/sf* |
| | 174 | 4.61 | 9.94 | 9.97 | −7.23 | −7.05 | $\alpha$70 | $\alpha$100 |
| | | | | | | −7.7* | | $\alpha$* |
| 116 | 174 | 4.27 | 10.83 | | −8.88 | −9.32* | $\alpha$ | $\alpha$* |
| | 176 | 3.44 | 10.75 | 10.71 | −8.68 | −8.42 | $\alpha$100 | $\alpha$ 100 |

region of transuranium nuclei [56–58] lead one to believe the accuracy of this type of calculation remains similar for SHE.

In Table I the theoretical results versus available experimental data and empirical evaluations [49,50,59] are shown. First, we give predicted values of quadrupole moments and then calculated and experimental $\alpha$-decay energies (columns 4 and 5) and decimal logarithms of total half-lives (in years) are displayed. Last, theoretical and experimental decay modes and intensities (in percentages) are given. It seems that the worst results for total half-lives is obtained for $^{256}$Fm where the disagreement of the measured and calculated values reaches 8 orders of magnitude. The predicted dominant decay mode is spontaneous fission, which is in agreement with experimental data. The other results differ from experimental ones on 2.4 orders of magnitude on the average, which is comparable with precision of earlier calculations of that type [22].

At present, for the heaviest nuclei only basic properties can be directly extracted from experiment (lifetimes and $Q_\alpha$ values). Ground-state masses cannot be obtained, thus the energies of emitted $\alpha$ particles are the only mass-type observables in this region. Standard error for $Q_\alpha$ energies resulting our calculations for SHE is 0.35 MeV. Although the

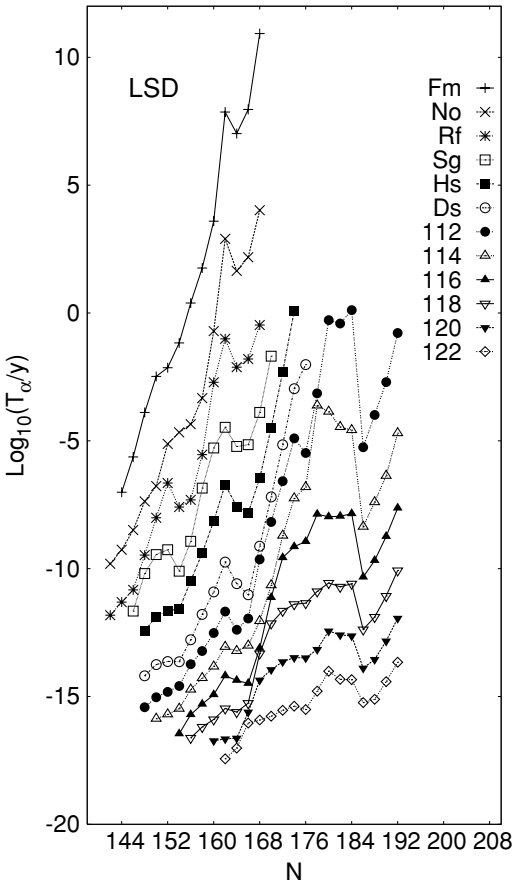


FIG. 11. Logarithms of $\alpha$-decay half-lives $T_\alpha$ (in years) obtained according to Viola-Seaborg formula Eq. (14).

nuclear masses in LSD model are determined with the average accuracy of about 0.7 MeV, the rms for $Q_\alpha$ in this region is highly satisfying.

## IV. SUMMARY

In the presented work we have compared four macroscopic models (Myers-Swiatecki drop, Yukawa-plus-exponential, droplet, and Lublin-Strasbourg drop) applied to determine global properties (static and dynamic) of heavy and superheavy even-even elements—from fermium up to $Z = 122$. Properties of about 210 nuclei were calculated and examined in macroscopic-microscopic approach in which the source of shell correction was the Woods-Saxon single-particle potential. Residual interactions were accounted in framework of BCS model where the pairing interaction was assumed to have constant matrix elements.

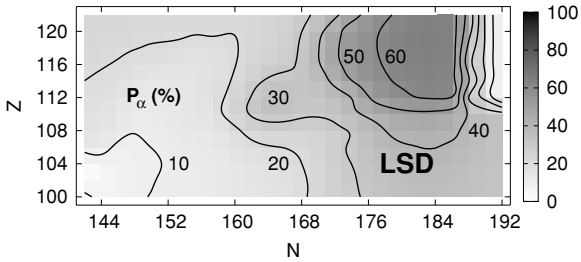


FIG. 12. Partial probability of $\alpha$-decay (in percentages) for SHE. The distance between isolines is 10%.

The research of SHE properties in this framework leads to a conclusion that MM models describe satisfactorily basic data of superheavies in a wide range of atomic and neutron numbers. The characteristics of nuclei with $Z \geqslant 116$ are predicted at the same level of accuracy. All models (in connection with WS potential) give comparable static properties (masses and $Q_\alpha$ values) but differ substantially in the case of dynamical quantities such as half-lives.

The quality of the reference model selected in the article, Lublin-Strasbourg drop, which has a relatively small number of free parameters fixed once for the whole periodic table of elements, is comparable to other discussed macroscopic models. $Q_\alpha$ energies are predicted with an average accuracy 0.35 MeV and logarithms of half-lives with the rms less than 2.5 orders of magnitude.

Based on these observations one can believe that the description of not only even but also of odd and doubly odd nuclei is promising as well. The latter is the subject of the forthcoming study.

## ACKNOWLEDGMENT

This work was partly supported by the Polish Committee for Scientific Research under Contract No. 1P03B13028.

[1] S. Hofmann, V. Ninov, F. Hessberger, P. Armbruster, H. Folger, G. Münzenberg, H. Schött, A. Popeko, A. Yeremin, A. Andreyev *et al.*, Z. Phys. A **350**, 277 (1995).
[2] S. Hofmann, V. Ninov, F. Hessberger, P. Armbruster, H. Folger, G. Münzenberg, H. Schött, A. Popeko, A. Yeremin, A. Andreyev *et al.*, Z. Phys. A **354**, 229 (1996).
[3] S. Hofmann, Nucl. Phys. **A616**, 370c (1997).
[4] B. Kalinkin, Y. Grabovskii, and F. Gareev, Acta Phys. Pol. **6**, 999 (1966).
[5] F. Gareev, B. Kalinkin, and A. Sobiczewski, Phys. Lett. **22**, 500 (1966).
[6] S. Nilsson, C. F. Tsang, A. Sobiczewski, Z. Szymański, C. Wycech, C. Gustafsson, I.-L. Lamm, P. Möller, and B. Nilsson, Nucl. Phys. **A131**, 1 (1969).
[7] Y. Oganessian, V. Utyonkov, Y. Lobanov, F. Abdullin, A. Polyakov, I. Shirokovski, Y. Tsyganov, G. Gulbekian, S. Bogomolov, B. Gikal *et al.*, Phys. Rev. Lett. **83**, 3154 (1999).
[8] Y. Oganessian, V. Utyonkov, Y. Lobanov, F. Abdullin, A. Polyakov, I. Shirokovski, Y. Tsyganov, G. Gulbekian, S. Bogomolov, B. Gikal *et al.*, Phys. Rev. C **63**, 011301(R) (2000).

[9] Y. Oganessian, V. Utyonkov, Y. Lobanov, A. Polyakov, I. Shirokovski, Y. Tsyganov, G. Gulbekian, S. Bogomolov, A. Mezentsev, S. Iliev *et al*., JINR Commun. **E7-2003-178**, (2003).
[10] K. Morita, K. Morimoto, D. Kaji, T. Akiyama, S.-I. Goto, H. Haba, E. Ideguchi, R. Kanungo, K. Katori, H. Koura *et al*., J. Phys. Soc. Jpn. **73**, 2593 (2004).
[11] S. Ćwiok, W. Nazarewicz, and P. H. Heenen, Phys. Rev. Lett. **83**, 1108 (1999).
[12] G. Lalazissis, M. Sharma, P. Ring, and Y. Gambhir, Nucl. Phys. **A608**, 202 (1996).
[13] M. Bender, K. Rutz, P.-G. Reinhard, J. Maruhn, and W. Greiner, Phys. Rev. C **60**, 034304 (1999).
[14] P. Möller, J. Nix, and K. Kratz, At. Data Nucl. Data Tables **66**, 131 (1997).
[15] I. Muntian, S. Hofmann, Z. Patyk, and A. Sobiczewski, Acta Phys. Pol. B **34**, 2073 (2003).
[16] A. Baran, Z. Łojewski, and K. Sieja, Eur. Phys. J. A **25**, s01, 611 (2005).
[17] A. Baran, Z. Łojewski, and K. Sieja, Acta Phys. Pol. B **36**, 1369 (2005).
[18] M. Sharma, G. Lalazissis, J. König, and P. Ring, Phys. Rev. Lett. **74**, 3744 (1995).
[19] A. Kruppa, M. Bender, W. Nazarewicz, P.-G. Reinhard, T. Vertse, and S. Ćwiok, Phys. Rev. C **61**, 034313 (2000).
[20] M. Sharma, A. Farhan, and G. Münzenberg, Phys. Rev. C **71**, 054310 (2005).
[21] I. Muntian and A. Sobiczewski, Phys. Lett. **B586**, 254 (2004).
[22] R. Smolańczuk, J. Skalski, and A. Sobiczewski, Phys. Rev. C **52**, 1871 (1995).
[23] R. Smolańczuk, Phys. Rev. C **56**, 812 (1997).
[24] R. Smolańczuk, Phys. Rev. Lett. **83**, 4705 (1999).
[25] W. D. Myers and W. J. Swiatecki, Ann. Phys. (NY) **84**, 186 (1974).
[26] H. J. Krappe, J. R. Nix, and A. J. Sierk, Phys. Rev. C **20**, 992 (1979).
[27] K. Pomorski and J. Dudek, Phys. Rev. C **67**, 044316 (2003).
[28] K. Pomorski and J. Dudek, Int. J. Mod. Phys. E **13**, 107 (2004).
[29] S. Ćwiok, J. Dudek, W. Nazarewicz, J. Skalski, and T. Werner, Comput. Phys. Commun. **46**, 379 (1987).
[30] W. Myers and W. Swiatecki, Nucl. Phys. **A601**, 141 (1996).
[31] W. D. Myers and W. J. Swiatecki, Ann. Phys. (NY) **55**, 395 (1969).
[32] P. Möller, J. Nix, W. Myers, and W. Swiatecki, At. Data Nucl. Data Tables **59**, 185 (1995).
[33] J. Berger, M. Girod, and D. Gogny, Nucl. Phys. **A428**, 23c (1984).
[34] H. Goutte, J. F. Berger, P. Casoli, and D. Gogny, Phys. Rev. C **71**, 024316 (2005).
[35] P. O. Fröman and N. Fröman, *JWKB Approximation, Contribution to the Theory* (North Holland Press, Amsterdam, 1965).
[36] S. Belyaev, Mat. Fys. Medd. Dan. Vid. Selsk. **30**, 11 (1959).
[37] S. Belyaev, Nucl. Phys. **24**, 322 (1961).
[38] A. Góźdź, K. Pomorski, M. Brack, and E. Werner, Nucl. Phys. **A422**, 26 (1985).
[39] M. Brack, J. Damgaard, H. Pauli, V. Strutinsky, and C. Wong, Rev. Mod. Phys. **44**, 320 (1972).
[40] J. Randrup, S. E. Larsson, P. Möller, S. G. Nilsson, K. Pomorski, and A. Sobiczewski, Phys. Rev. C **13**, 229 (1976).
[41] S. Ćwiok and A. Sobiczewski, Z. Phys. A **342**, 203 (1992).
[42] R. Smolańczuk, H. Klapdor-Kleingrothaus, and A. Sobiczewski, Acta Phys. Pol. B **24**, 685 (1993).
[43] A. Baran, K. Pomorski, A. Łukasiak, and A. Sobiczewski, Nucl. Phys. **A361**, 83 (1981).
[44] V. Viola and G. Seaborg, J. Inorg. Nucl. Chem. **28**, 741 (1966).
[45] Z. Patyk and A. Sobiczewski, Nucl. Phys. **A533**, 132 (1991).
[46] J. Dudek, A. Majhofer, and J. Skalski, J. Phys. G **6**, 447 (1980).
[47] Z. Patyk, J. Skalski, A. Sobiczewski, and S. Ćwiok, Nucl. Phys. **A502**, 591c (1989).
[48] S. Hofmann, F. Hessberger, D. Ackerman, G. Münzenberg, S. Antalic, B. Cagarda, P. Kindler, J. Kojuharova, M. Leino, B. Lommel, R. Mann *et al*., Eur. Phys. J. A **14**, 147 (2002).
[49] G. Audi, O. Bersillon, J. Blachot, and A. Wapstra, Nucl. Phys. **A729**, 3 (2003).
[50] G. Audi, A. Wapstra, and C. Thibault, Nucl. Phys. **A729**, 129 (2003).
[51] H. Lipkin, Ann. Phys. (NY) **9**, 272 (1960).
[52] Y. Nogami, Phys. Rev. **134**, B313 (1964).
[53] A. Baran, Z. Łojewski, and K. Sieja, in preparation.
[54] Z. Łojewski, A. Baran, and K. Pomorski, Acta Phys. Pol. B **34**, 1801 (2003).
[55] S. Goriely, J. Pearson, and F. Tondeur, At. Data Nucl. Data Tables **77**, 311 (2001).
[56] I. Muntian, Z. Patyk, and A. Sobiczewski, Yad. Fiz. **66**, 1051 (2003).
[57] Z. Łojewski and A. Baran, Z. Phys. A **329**, 161 (1988).
[58] A. Staszczak, S. Piłat, and K. Pomorski, Nucl. Phys. **A504**, 589 (1989).
[59] Y. Oganessian, V. Utyonkov, Y. Lobanov, F. Abdullin, I. Shirokovski, Y. Tsyganov, G. Gulbekian, S. Bogomolov, B. Gikal, A. Mezentsev *et al*., Phys. Rev. C **69**, 054607 (2004).